



Unraveling the Nature of Weak Hydrogen Bonds and Intermolecular Interactions Involving Elements of Group 14–17 via Experimental Charge Density Analysis

T. N. Guru Row* 

Abstract | Mapping of charge densities in molecular crystals has been contemplated ever since it was recognized that X-rays are scattered by the electron density in the crystal. The methodology both from the experimental and theoretical perspective was standardized and applied extensively only during the last few decades, as technological advances were a prerequisite in both data collection and computation. Multipole formalism developed for accurate X-ray diffraction data is routinely utilized in conjunction with the concept of atoms in molecules to obtain quantitative estimates of the topological properties in molecular crystals which allow the evaluation of both bonded and non-bonded contacts. Recently, with the advent of quantum crystallography, combining Hirshfeld atom refinement along with libraries of extremely localized molecular orbitals, HAR-ELMOs, has emerged as an alternate approach. Apart from the weak hydrogen bonds, other highly directional non-bonded contacts like halogen, pnictogen, chalcogen and carbon bonds have been subjected to charge density analysis to experimentally observe and quantify σ -holes using experimental high-resolution X-ray diffraction data. The recognition of lack of directional preferences in hydrophobic interactions is demonstrated experimentally which might have far reaching consequences in the areas of materials and biology.

1 Introduction

Non-bonded contacts less than the sum of van der Waal radii of the participating atoms define the presence or absence of intra- and intermolecular interactions and in case of molecular crystals define the strength and directionality of such interactions. This forms the basis of crystal engineering¹ and the definitions of hydrogen bond and halogen bond have emerged from the IUPAC committees in recent years based on distance and angle criteria. However, it needs to be recognized that though these are only qualitative estimates, though considered enough by the practicing crystal engineering community and with the rich information available from X-ray diffraction

studies, it is now an appropriate time to obtain quantitative insights into all types of non-bonded contacts. This will energize crystal engineering tools to design and fabricate the desired properties in futuristic materials.

Design and fabrication of new solids with desirable physical and chemical properties have dominated the area of materials with an emphasis on the chemical synthesis of representative model compounds to generate required packing modes of molecules with specific interactions in a crystalline framework. Crystal engineering aims at the understanding of intermolecular interactions and hopes to design materials with the required properties. In their review on ‘Chemical applications

¹ Solid State and Structural Chemistry Unit, Indian Institute of Science, Bangalore 560012, India.
*gururrow@iisc.ac.in

of X-ray charge density analysis', Koritsánszky and Coppens² concluded that 'X-ray charge density analysis has grown into a mature field and, like in the development of structure determination, the methods have been standardized to a large extent so that more routine use can become possible.' They remarked that a parallel analysis of theoretical results of both isolated molecules and periodic crystals is becoming increasingly common leading to an analysis of the changes in molecular properties in a crystal. McKinnon et al.³ showed that using Hirshfeld surfaces to partition crystal space, packing modes and intermolecular interactions in molecular crystals can be visualized apart from getting a quantitative measure in terms of relative strength involved in casting molecular species into the crystal lattice. Krawczuk and Macchi in their review⁴ conclude that 'in the future, one may expect that the whole process of material design and fabrication could be integrated, having as initial step predictions based on calculated or measured electron density models of the molecular building blocks, that could offer an initial guess of the expected property of a crystalline solid'.

X-ray diffraction technique for mapping the charge density distribution in crystals is the preferred methodology, as the X-rays are mainly scattered by the total electron density in a crystal. Recent technological advances made in instrumentation allow the accumulation of high-accuracy X-ray diffraction data in quick time and along with the advances made in the area of computation it is now possible to compare the best charge density extracted from experiment with those obtained from theory. Structures determined from routine X-ray diffraction techniques allow for the identification of intermolecular interactions and, with accurate data sets followed by a charge density mapping, information on net charge transfer in different components of the molecule can be analyzed. In this context, the most popular Hansen and Coppens multipolar formalism⁵ incorporated in the package XD⁶ is utilized for mapping the deformation densities due to chemical bonding. Calculation of one-electron properties is facilitated via multipole refinements of experimental structure factors assisted by topological analysis of the derived electron density and evaluation of the atomic basin properties. Quantum chemical calculations provide the generation of accurate wave functions for chemically interesting species. Several powerful computer programs, e.g., Gaussian⁷, provide high-level *ab initio* wave functions for a fairly complex molecule. However, it must be

mentioned that the charge density distributions from experimental methods, despite considerable effort and time, automatically incorporates correlated motion of electrons, a feature of enormous significance in molecular crystals. In this context, the computer program developed over the years from the group at Torino CRYSTAL 17⁸ allows single point periodic calculations based on a given geometry using different methods, e.g., HF or density functional theory (DFT) inclusive of electron correlation. Using the density-based quantum theory of atoms in molecules (AIM), established as the most powerful tool to analyze and interpret the charge densities obtained from both experiment and theory, topological parameters and descriptors of bonding characteristics can be derived. The identification of critical points (CP) where the gradient of the electron density vanishes, the mapping of bond paths (BP), which trace the inter-nuclear distance, the Laplacian of the electron density, which brings out the nature of intra- and intermolecular interactions are some of the directly derived properties from the AIM analysis. It should be pointed out that the limitations of multipole model due to poor representation of heavier atoms and polar bonds puts severe restrictions on the extension of the methodology to futuristic functional materials. Jayatilaka proposed the X-ray wave function (XCW)⁹ fitting based on atomic positions and anisotropic displacement parameters (ADPs) resulting from a Hirshfeld atom refinement (HAR)¹⁰ as an alternate to multipole refinement. It is to be noted that due to the availability of full reconstructed density matrix in X-ray wave function refinement, this approach is capable of handling various chemical problems, such as experimentally derived bond order and electron pair localization. Grabowsky and Ginoni proposed a new quantum crystallographic method, HAR–ELMOs coupling, i.e., the crystallographic refinement method Hirshfeld atom refinement (HAR) combined with the recently constructed libraries of extremely localized molecular orbitals (ELMOs)¹¹.

Quantum crystallography brings out two major areas of modern science, quantum chemistry and crystallography into a single integrated methodology which allows the determination of structure–property correlation at the electronic level thus suggesting an unambiguous pathway for targeted materials design. The key components are the synthesis, structure determination, mapping the charge densities from experiment on one hand and combining the quantum chemical method-based theoretical estimates with

modeling on the other. Diffraction and scattering experiments are intimately connected with quantum chemical methods, as the former provides structures of molecules or polyatomic ions at atomic level while the latter derives wave functions and properties from them. The first definition of quantum crystallography came from the work of Massa et al.¹² and the implementation of quantum crystallography was demonstrated in the seminal work of Clinton and Massa¹³. Other pioneering quantum crystallography methods include X-ray atomic orbital (XAO) method developed by Tanaka et al.¹⁴. Using this method, they determined atomic orbitals on transition metal ions. The results of the XCW fitting⁹ depend on the quality of positional and thermal parameters and the model through which these are obtained [i.e., independent atom model (IAM), multipole model (MM), Hirshfeld atom refinement (HAR)]. The initial step of HAR¹⁰ requires a set of atomic coordinates, either obtained from a spherical or an aspherical atom refinement to calculate a molecular wave function of the molecule/molecules (asymmetric unit) using standard self-consistent field (SCF) method. A first electron density (ED) corresponding to the asymmetric unit is calculated from this quantum mechanical wave function. This electron density is divided up into aspherical atomic densities using Hirshfeld partitioning scheme. The charges and moments of these atoms are calculated and used to simulate the electric field surrounding the molecule of interest. A new electron density is then calculated in the presence of the simulated crystal field. These cycles, also known as electron density cycles are repeated to convergence in the molecular energy resulting in what is termed as an electron density step. Subsequently, the Fourier transforms of the new aspherical atom electron densities are used as non-spherical atomic scattering factors in a conventional crystallographic least-squares refinement of the coordinates and ADPs. This step, called a structural refinement step, consists of several least-squares cycles in a conventional crystallographic refinement. The sequence of an electron density step followed by a structural refinement step is called a 'HAR iteration'. These iterations are repeated until both electron density cycles and refinement cycles show no further changes.

In this mini-review, I intend to give an overview of the charge density methodology and illustrate its versatility by citing examples from the work carried out over the last few years in our group concerning quantitative evaluation of intermolecular interactions involving elements

in Group 14: the tetrrels (carbon family), Group 15: the pnictogens (nitrogen family), Group 16: the chalcogens (oxygen family) and Group 17: the halogens (fluorine family) of the periodic table. The polarizability concept of atoms (σ holes) in these groups decides the highly directional nature of interactions and provides the basis for molecular assemblies in crystal lattices. In this context, the nature of hydrophobic interactions makes an interesting deviation.

2 Elements of Experimental Electron Density Determination

The basis of X-ray structure analysis is the assumption that the atomic electron density is essentially the spherically averaged density of an isolated atom. This allows for considering the molecular crystal to be built up by spherical independent atoms, which bond together into a molecule, which then rearranges following the allowed symmetry in the crystal lattice as a molecular crystal. The independent atom model (IAM) assumes that the atoms in a crystal are neutral. It must be mentioned that the success of the spherical atom model has been witnessed in terms of the extensively large number of crystal structures that have been determined based on this assumption, suggesting that the electron density deformation on bond formation is a very minimal fraction compared to the overall density at the atomic center.

$$\rho_{\text{IAM}}(r) = \sum_k \rho_k^{\circ}(r - R_k).$$

This equation retains the electrons localized around a nucleus and further assumes that the electron density in the molecule (and eventually in the crystal) is a superposition of isolated spherical densities ρ_0 of isolated atoms k centered at R_k . The thermal smearing is again restricted to the atom center and the mean square atomic displacement is expressed in terms of either harmonic or anharmonic parameters. Further, the Fourier transform leads to the generalized structure factors,

$$F(H) = \sum_k f_k(H) \exp(2\pi^2 H' U_k H) \exp(2\pi i H R_k^0).$$

The IAM is effective for heavy atoms with dominant core scattering, whereas in lighter atoms the directional characteristics of bonding features like valence become more and more aspherical which leads to properties such as the dipole moment and higher electrostatic

moments exhibited by molecular crystals. The limitations of IAM are thus inadequate to describe the scattering from covalently bonded crystals as observed in the case of diamond, the appearance of the space group forbidden 222 reflection and the anomalously high intensity of the 100 reflection in the powder diffraction pattern of graphite. Further, theoretical and experimental evidence showing that atoms in molecules carry partial charges necessitated improvement in the IAM. The first extension of IAM to allow for both valence charge transfer and expansion/contraction of the valence shell was suggested by Coppens et al., now called the radial (κ , κ') refinement strategy¹⁵. Various groups introduced several aspherical correction terms, but the multipole expansion model suggested by Hansen and Coppens⁵ has stood the test of time and is now the most widely used methodology. In this model, the individual atomic densities are divided into three components, the core, spherical expansion and contraction term (κ) in the valence shell and the valence deformation in terms of density-normalized spherical harmonics ($d_{lm\pm}$) together with the corresponding radial expansion and contraction (κ') of the valence shell as given below,

$$\rho_{\text{at}}(r) = \rho_{\text{core}}(r) + P_{\text{v}}\kappa^3\rho_{\text{valence}}(\kappa r) + \sum_{l=0}^{l_{\text{max}}} \kappa'^3 R_l(\kappa' r) \sum_{(m=0)}^l P_{lm\pm} d_{lm\pm}(\theta, \varphi).$$

ρ_{core} and ρ_{valence} represents the spherical atomic scattering factors derived from ground-state Hartree–Fock wave functions which are tabulated in various databases. If P_{c} is the spherical core defined under ρ_{core} , then P_{v} is the spherical valence population parameter. P_{v} provides a rough estimation of the net atomic charge by $q = N_{\text{v}} - P_{\text{v}}$, where N_{v} is the number of valence electrons in a free neutral atom. The aspherical valence density is expressed in terms of $d_{lm\pm}$, the density-normalized spherical harmonics of degree l and order m . $P_{lm\pm}$ denotes multipole populations and $R_l(r)$ are the Slater-type radial functions. The coefficients κ and κ' describe the contraction–expansion of spherical and multipolar valence densities, respectively. The radial function R_l in the deformation valence density is based on single-zeta Slater-type orbitals with energy-optimized exponents ζ taken from valence-orbital wave function calculations.

$$R_l(r) = \frac{\xi nl + 3}{(nl + 2)!} (r)^{n(l)} \exp(-\xi r).$$

It is noteworthy that the multipole modeling provides the primary source of chemical information from the X-ray diffraction experiment beyond pure geometry. The total electron density distribution is calculated based on $F(H)$, the structure factor, by the Fourier transformation as:

$$\rho(r) = \int F(H) \exp(-2\pi H \cdot r) dH.$$

The difference between the observed and the calculated electron density is called residual density. This is a representation of the inadequacy of the multipolar modeling and is evaluated as follows:

$$\Delta\rho(r) = \rho_{\text{obs}}(r) - \rho_{\text{calc}}(r) = \frac{1}{V} \sum_H \Delta F \exp(2\pi i H \cdot r).$$

The deformation density, the difference between the total density and the density calculated based on the promolecule density is a representation of valence density into the bonding regions and can be expressed as:

$$\Delta\rho(r) = \rho(r) - \rho_{\text{pro}}(r).$$

If the observed structure factors are used, the resulting electron density map is called a dynamic deformation density map, since the observed structure factors include thermal effects. The static deformation density map is free from thermal smearing effects and can be directly compared with theoretical deformation density.

3 Instrumentation for Charge Density Analysis

High-quality X-ray data are of primary importance for charge density modeling as compared to routine crystal structure determination. Therefore, the availability of good quality single crystals without any twinning and disorder is extremely desirable. Further, charge density analysis demands high-resolution X-ray data [preferably $(\sin\theta/\lambda)_{\text{max}} > 1.1 \text{ \AA}^{-1}$] to deconvolute thermal motion and electron density (more specifically bonding features). To get the sufficient number of intense high-order reflections, and to minimize thermal motion, the crystal should be cooled to lowest possible temperature using either nitrogen or helium cryogenics. In-house X-ray sources such as microfocus sealed tubes and rotating anode sources coupled to multilayer X-ray optics augments the X-ray flux density to an enormous extent. Subsequently, data collection times are reduced from weeks to days and studies on weakly diffracting sample are also possible. On

the other hand, synchrotron radiation scores over laboratory X-ray diffractometer in many aspects such as tunable wavelengths, higher intensity and shorter data acquisition time. Higher intensity allows use of smaller crystals for data collection, thereby reducing crystal absorption and extinction problems. Apart from reliable synchrotron data, significant improvements in data treatment software for synchrotron data have made the charge density method competent in analyzing complex and challenging systems including macromolecules. Use of advance detector system to measure scattered radiation like CCD, CMOS, IP and XPAD (Pilatus) has ensured high quality in measurements of diffraction intensities with high signal-to-noise ratios. It must be mentioned that parallel developments in storage and high speed in computers allow for high-level theoretical calculations to facilitate comparisons with the experimental results.

4 Topology of Electron Density and Bonding Descriptors

The electron density modeled either from multipole formalism or quantum crystallography does not explain the nature of chemical bonding in molecules, especially the mechanism of electron sharing between atoms. Thus, the electron density must be subjected to Bader's quantum theory of "Atoms in Molecules" (AIM) approach¹⁶. This approach allows the interpretation of a detailed topological analysis of charge distribution for the understanding of chemical and physical properties. QTAIM exploits charge density or electron density of molecules $\rho(r)$ as a meaningful tool to study the nature of bonding in molecular systems. The topological properties of electron density and its derivatives are useful in defining the concept of bonding through bond paths and bond critical points (BCPs). A bond is generally characterized by a bond path (R_{ij}), which defines a maximum density path connecting the two bonded atoms. The point on the path at which the gradient of electron density is zero, $[\nabla\rho(r_c)=0]$ is the bond critical point (BCP). The sign of second derivative of electron density, the Laplacian, at this point determines whether the function is a maximum or a minimum (Fig. 1).

In general, the theory of AIM provides a methodology for the identification of a bond between any two atoms in a molecule in terms of CP, called bond critical points (BCPs). This analysis is based on the identification of CP, classified using the Hessian matrix of the electron density which is a 3×3 ordered array of the second

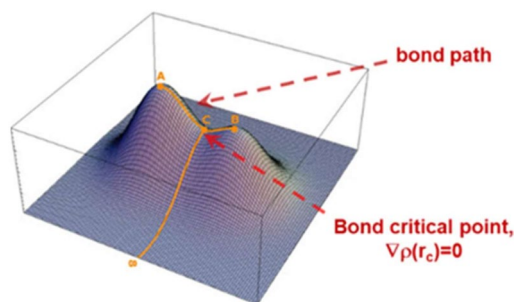


Figure 1: Topology of bonding density between atoms A and B. (diagram reproduced from the website, <http://www.ruudvisser.com/publications/talks/>)

derivatives of $\rho(r)$. The Hessian matrix generates three eigenvectors, which are mutually orthogonal and coincide with the so-called principal axis of curvature. This suggests that each eigenvector represents an axis and the corresponding eigenvalues (λ_1, λ_2 and λ_3 with $\lambda_1 \leq \lambda_2 \leq \lambda_3$) determines the profile of the electron density along this axis. The number of non-zero curvatures of the Hessian matrix defines the rank associated with the CP and the signature of a CP is the sum of the signs of the curvatures and in general, a CP is labeled by giving both its rank and signature. It is noteworthy that the CPs in a stable molecule are all of rank 3, which gives rise to four possible types of CPs (Fig. 2):

(3, - 3) Peaks: all curvatures are negative and are a local maximum at r_c (effectively the position of the nuclei). It may be mentioned that recently non-nuclear attractors (NNAs) have been identified to possess (3 - 3) critical points in Li clusters

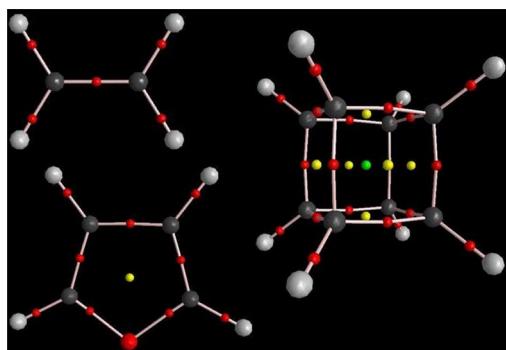


Figure 2: Types of critical points: (3, - 3) non-nuclear critical point (dark and light gray). Red dot (3, - 1) bond critical point, yellow dot (3, + 1) ring critical point, while (3, + 3) is the cage critical point (green). (Sounak Sarkar, PhD thesis).

(3, - 1) Passes or saddle points: two negative and one positive curvatures; $\rho(r_c)$ is a local maximum along two of the axes and a local minimum along the third orthogonal axis, found between every pair of nuclei linked by a chemical bond. These are referred to as bond critical points (BCPs)

(3, + 1) Pales: two positive and one negative curvatures; $\rho(r_c)$ is a local minimum along two of the axes and a local maximum along the third orthogonal axis, found at the center of a ring of bonded atoms. These are referred to as ring critical points.

(3, + 3) Pits: all three curvatures are positive and a local minimum at r_c . These are referred to as cage critical points.

For intermolecular interactions, the CPs of the type (3, - 1), and the properties of $\rho(r)$ at these points provide the most useful information chemically and are of great interest. The line of the highest electron density linking any two atoms is referred to as the bond path and its length R_{ij} (need not be the same as inter-atomic vector) is referred to as the interaction length, which passes through the BCP. The existence of a (3, - 1) CP and associated BP provides the topological definition of a chemical bond. For strained systems, the BPs deviate from the inter-nuclear vectors. If the charge is preferentially accumulated in a particular plane along the BP, the bond will no longer be cylindrical, rather it will have an elliptical cross-section ($\lambda_1 \neq \lambda_2$). A quantitative measure of the ellipticity of a bond, bond ellipticity is defined as $\varepsilon = \lambda_1/\lambda_2 - 1$, where λ_2 is the curvature of smaller magnitude. The strength of a bond or the bond order is defined by the magnitude of the charge density at the BCP, ρ_b . An important function of (r) is the second derivative, the Laplacian $\nabla^2\rho(r)$, a scalar quantity and defined as the sum of the principal curvatures ($\lambda_1 + \lambda_2 + \lambda_3$), it is a representation of the chemical features of the molecule. The physical significance of the Laplacian is that it represents areas of local charge concentration and depletion. If $\nabla^2\rho(r) < 0$, the density is locally concentrated resulting in shared interactions, whereas in the case of $\nabla^2\rho(r) > 0$, the electron density is depleted representing closed-shell interactions. It is possible to observe lone pairs in the Laplacian as these appear as local maxima, i.e., (3, - 3) CPs in the negative Laplacian. The electron density, Laplacian, interaction line, the curvatures, and the bond ellipticity together represent the topology of the charge density distribution of a given molecule.

5 Definition of Intermolecular Interactions, Hydrogen Bonds and Crystal Engineering

One of the most significant factors in molecular crystals is the optimized arrangement of molecules in the crystal lattice. A subtle interplay of molecular recognition on one hand and the symmetry in the lattice on the other dictate the packing modes. Intermolecular interactions of varying strengths act in tandem to provide the best choices for minimum energy configuration governed by symmetry restraints in a crystalline lattice. Indeed, these features allow for different packing modes among crystals leading to the occurrence of polymorphism. In the last few decades, systematic analysis based on results derived from the Cambridge Structural Database have generated several well-identified patterns, called synthons^{1, 17–19}, which act as the basic tools in crystal engineering heralding a major component in chemical crystallography. Crystal engineering has clearly brought out the importance of recognizing patterns found by intermolecular interactions. For H-bonds, several approaches have been suggested and the method of Etter²⁰ has paved the way for characterizing H-bonds in terms of predefined motifs like ribbons, tapes, and loops. The approach to use CSD to view intermolecular interactions, e.g., H-bond parameters in terms of crystal correlations studies, has come to be recognized as a powerful tool to gain insights into weak and strong H-bonds. A working definition for hydrogen bonds states ‘A hydrogen bond exists between XH and an atom (or group of atoms) A, if the interaction between XH and A (1) is bonding and (2) sterically involves the hydrogen bond.’²¹ A major concern in such a definition comes from the fact that strong H-bonds have nearly covalent interactions, while weaker H-bonds are generally electrostatic in nature. In fact, there has been no experimental proof for a critical distance at which the H-bond switches to van der Waals type. Koch and Popelier have proposed eight criteria, which need to be satisfied to ensure the formation of a H-bond based on theoretical charge density distributions between H and A²². A possible ‘region of overlap’, which allows for the switching from an H-bond to van der Waals type has been identified, based on the charge density analysis of coumarin and two of its derivatives from both experiment and theory²³. A path-breaking charge density-based analysis, to categorize strong and weak H-bonds, has been reported recently by Mallinson et al.²⁴, which indicates ‘a Morse-like dependence of

the Laplacian of $\rho(r)$ on the length of interaction line, which allows a differentiation of ionic and covalent bond characters'. The strength of the interactions studied varies systematically with the relative penetration of the CPs into the van der Waals spheres of the donor and acceptor atoms, as well as on the interpenetration of the van der Waals spheres themselves. In a seminal article, Munshi and Guru Row²⁵ evaluated intermolecular interactions in terms of both experimental and theoretical charge density analyses to produce a unified picture with which to classify strong and weak hydrogen bonds, van der Waals interactions, into three regions. It is clear from these studies that quantification and classification of weak and strong intermolecular interactions in terms of their strength and directionality can be achieved unequivocally via charge density analysis.

6 Politzer's Sigma (σ) Hole Concept

A σ -hole bond is a non-covalent interaction between a covalently bonded atom of Groups 14–17 and a negative site, e.g., a lone pair of a Lewis base or an anion²⁶. When the atom forms a covalent bond, some of its electronic charge is polarized toward the bond region, leading to the atom's electronic density being diminished in its outer region (along the extension of the bond) but increased on its equatorial sides (Fig. 3). The consequence is that a negative electrostatic potential develops around the sides of the atom which signifies the lone pairs, while on the extension of one of the covalent bonds to the atom, a region of positive electrostatic potential, labeled as σ -hole gets developed. The interaction of the nucleophile with this positive σ -hole gives rise to highly directed non-covalent bond. The σ -hole features become more prominent with the increase in polarizability and decrease in electronegativity of atom. Recent efforts in high-resolution X-ray

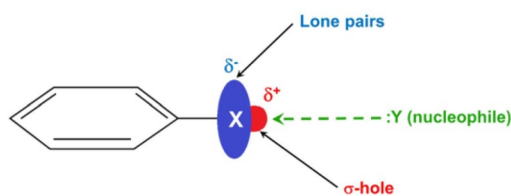


Figure 3: Regions of positive σ -hole and negative lone pairs highlighting the anisotropy associated with the electron density distribution around the covalently bonded X atom. The σ -hole interacts with nucleophile to form a highly directed non-covalent bond.

charge density analyses have made it possible to experimentally visualize the theoretically predicted anisotropic electron density distribution and hence the “ σ -holes” on the Groups 14–17 atoms as shown later in the illustrated examples.

7 Halogen Bonding

Halogen bond defines a specific subgroup of inter- and intra-molecular interactions involving a halogen atom in a molecular self-assembly. A typical halogen bond is denoted as $Y-X\cdots D$, where $Y-X$ is the halogen bond donor, X is any halogen atom with an electrophilic (electron-poor) region, and Y is a group covalently bound to X and D is the halogen bond acceptor and is typically a molecular entity possessing at least one nucleophilic (electron-rich) region. “A halogen bond occurs when there is evidence of a net attractive interaction between an electrophilic region associated with a halogen atom in a molecular entity and a nucleophilic region in another, or the same, molecular entity” as defined by the IUPAC task group recently (Fig. 4)²⁷.

Early studies on molecular complexes of Br_2 with several oxygen containing organic compounds identified halogen atoms as recognition sites in self-organization by specific $Br\cdots O$ interactions. In recent times, the formation of halogen bonds has been extensively utilized in (i) designing organic functional materials, (ii) separation of enantiomers, (iii) self-assembly of supramolecular liquid crystals, (iv) generating polymorphic phases, and (v) in the formation of polymers. In addition, halogen bonds have gained enormous importance in biology due to the selective binding of small molecules to receptors where the molecular recognitions are mediated through such bonds.

8 Halogen \cdots Halogen Interactions

Halogen \cdots halogen interactions are a special class of halogen bonds where both the bond donor and acceptor are halogen atoms. They have been referred in literature by various names, such as “donor–acceptor”

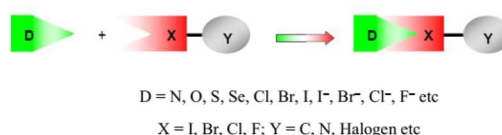


Figure 4: Schematic representation of donor/acceptor sites in a halogen bond.

interactions, “secondary” interactions, “charge transfer” interactions and interactions between the highest occupied molecular orbitals and the lowest unoccupied molecular orbitals (HOMO–LUMO). Halogen•••halogen ($X\cdots X$) contacts in molecular crystals have been a topic of interest mainly regarding the attractive or repulsive behavior of the interaction between two identical atoms. The “anomalous halogen atom contacts” was explained by Williams and Hsu²⁸ for $\text{Cl}\cdots\text{Cl}$ interactions to be around 3% of the energy of a $\text{Cl}\text{--}\text{Cl}$ covalent bond. Nyburg and Wong-Ng²⁹ assigned anisotropic non-bonded radii to Cl atoms in crystals. Based on Cambridge Database analysis, Desiraju and Parthasarathy³⁰ concluded that $\text{Cl}\cdots\text{Cl}$, $\text{Br}\cdots\text{Br}$ and $\text{I}\cdots\text{I}$ interactions are highly attractive (and anisotropic) in nature, whereas $\text{F}\cdots\text{F}$ interactions do not have any additional stabilizing role in close packing of the crystals. It was observed that $X\cdots X$ contacts adopt one of the two interaction geometries, type I or type II (Fig. 5), Type I ($\theta_1 \approx \theta_2$) contacts are subdivided further into *cis* and *trans* depending upon the relative positions of the interacting atoms with respect to the symmetry elements (*cis* across the rotation axis and *trans* across the inversion center). Type II contacts are found between molecules related through screw axes and glide planes. Using Politzer’s ‘ σ -hole’ concept, the electrostatic nature of halogen•••halogen interactions has been understood where the charge depletion (CD) region (i.e., a positive σ -hole site) of one of the halogens approaches the charge concentration (CC) region (a negative belt) of the other.

9 Pnicogen Bond

Pnicogen bond is a non-covalent bond formed between Group 15 element as an electron-pair acceptor and a nucleophile. In a typical pnicogen bond, the lone pair of the donor atom faces the ‘ σ -hole’ on the pnicogen atom and hence is highly directional in nature and sensitive to angular distortion compared to typical hydrogen bonds. This is mainly due to exchange repulsion, a factor that arises due to steric repulsion between electron clouds on the nucleophile and the electrophile.

10 Chalcogen Bond

Elements of the Group 16 form intermolecular contacts apart from hydrogen bonding akin to the halogen bonds. Rosenfeld et al.³¹ reported the directional preferences of interactions involving sulfur. Guru Row and Parthasarathy³² showed the involvement of electrophile–nucleophile nature in $\text{S}\cdots\text{S}$ interactions invoking the concept of anisotropy in the otherwise spherical nature of the Sulfur atom thus invoking the future definition of the σ -hole concept. Chalcogen bonding attained its importance soon after the discovery of organic conducting materials involving sulfur.

11 Carbon Bond

Among the non-covalent interactions other than the well-explored classes of hydrogen bonding, non-canonical interactions such as halogen bonding, chalcogen bonding and pnicogen bonding are of electrostatic origin. Though these non-covalent interactions have been known to exist for several years, the description based on the formation of ‘ σ -holes’ on the donor atoms

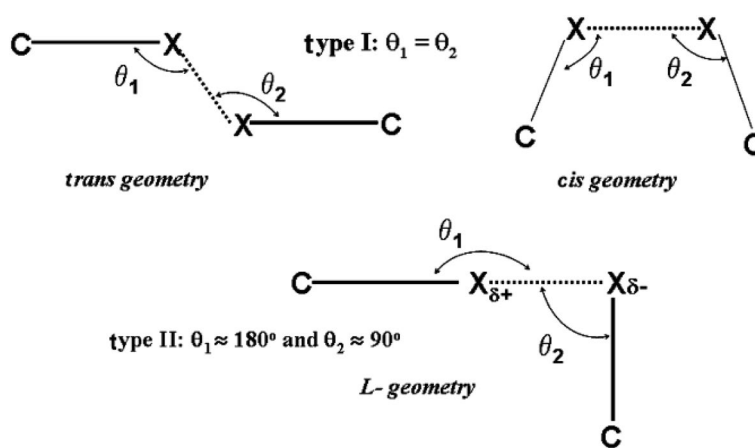


Figure 5: Schematic representation of the type I (*trans* and *cis* geometry) and type II (L-geometry) halogen•••halogen contacts.

was demonstrated by Politzer et al.²⁶ Indeed, their studies on compounds containing Group 14 elements such as Si and Ge also show similar behavior. Mani and Arunan³³ in their recent seminal paper suggested that the carbon atom, the most commonly occurring element belonging to the Group 14, in fact could act as an electrophilic center which can non-covalently bond with nucleophilic atoms, leading to ‘carbon bonding’ (following a nomenclature analogous to the halogen–chalcogen bonding).

12 C–H...O Hydrogen Bonds, Intermolecular Interactions Involving Elements in Group 14–17 and Hydrophobic Interactions

As indicated earlier, the focus of this mini-review is to illustrate with examples taken from the work done in our group on the charge density analysis over the last few years bringing out the salient features of the bonding descriptors derived from experimental studies. The role of multifaceted C–H...O hydrogen bonds in stabilizing the structure of ferulic acid, the role of the enigmatic “fluorine” in halogen bonding, chalcogen bonding in acetazolamide, a diuretic drug using the quantum crystallographic methodology, first experimental proof for the pnictogen bond in the structure of a cocrystal of 2-amino-5-nitropyridine with 2-chloroacetic acid, the proof for the occurrence of the carbon bond, and finally the group...group interactions in hydrophobic interactions will be briefly presented in the following sections. These examples firmly establish that experimental and theoretical charge density analyses are essential to bring out the quantitative properties of intermolecular interactions to aid in the design of materials. Only the key features of the charge density analysis results relevant to the respective intermolecular interactions are listed with illustrations and tables from the publications (Fig. 6).

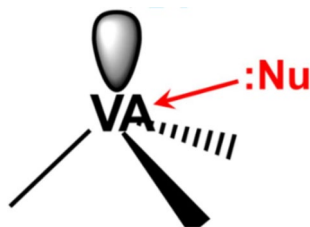


Figure 6: Schematic representation of pnictogen bond between a group 15 (VA) element and a nucleophile (:Nu); reproduced from thesis of Dr. Sounak Sarkar, IISc.

13 Hydrogen Bonding in Ferulic Acid: The Gulliver Effect

The description and authentication of C–H...O interactions as a weak hydrogen bond and also as an essential crystal engineering element have been highlighted in several reviews and text books³⁴. The reported crystal structure of ferulic acid earlier identified the presence of strong O–H...O hydrogen-bonded dimers dominating the packing in the crystal structure (Fig. 7). In addition, the structure offers a case for trifurcated C–H...O hydrogen bonding environment and allows for an evaluation of the topological features of such a system. The topological properties derived from the experimental and theoretical charge density analysis on ferulic acid provide insights into the electrostatic nature of trifurcated weak hydrogen bonds with respect to the lone pair directionality associated with the acceptor oxygen atom. The contribution of electrostatic component is evident in the interaction energies calculated by the EPMM method³⁵ and in the electrostatic potential surfaces. The topological properties of all intermolecular interactions and the interaction energies are given in Tables 1 and 2. Interestingly, interaction energies quantify that a group of weak interactions can conjointly match or even surpass the strength of a strong classical hydrogen bond thus resulting in what is termed as the Gulliver effect³⁶.

14 The Role of the Enigmatic “Fluorine” in Halogen Bonding

Fluorine is a curious element in the periodic table raising questions on its ability to form intermolecular interactions, because it is the most electronegative element and is the smallest and least polarizable halogen atom. However, fluorine interactions appear ubiquitously in compounds of relevance to pharmaceutical and organic functional materials, the most common being the C–H...F hydrogen bond. But other intermolecular interactions involving fluorine which are debated mainly include the halogen bond³⁷. It is well established that the halogen behaves as a donor (electrophilic) towards an acceptor (nucleophile) atom in a typical halogen bond, where the electrophilic site on the halogen is termed as a “σ-hole”. Recent theoretical and experimental charge density studies suggest the possibility of polarization of the electron cloud in fluorine^{38, 39}. The enigmatic type II C–F...F–C and C–F...S–C interactions in pentafluorophenyl 2, 2′-bithiazole are shown to be realistic “σ-hole” interactions

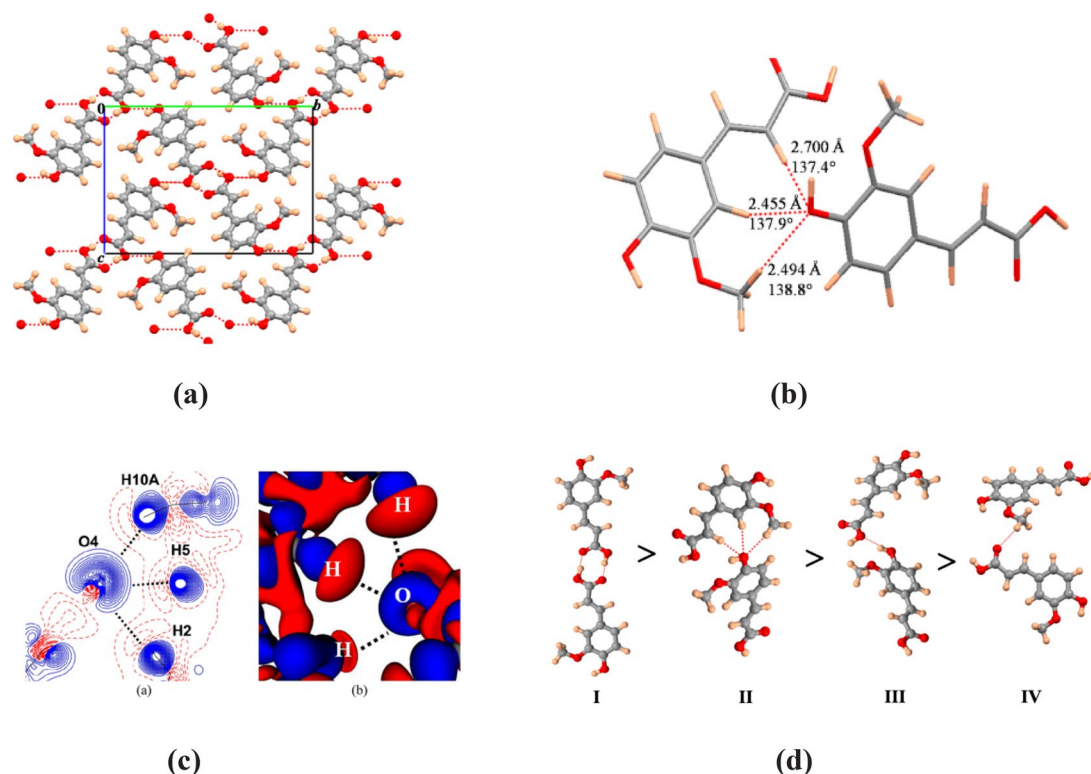


Figure 7: **a** Packing diagram showing the prominent O–H...O dimers, **b** the resulting trifurcated C–H...O interactions. **c** 2D and 3D static deformation density map generated from the experimental model showing the trifurcated C–H...O hydrogen bond region, **d** molecular dimers formed by (I) O–H...O (carboxylic) hydrogen bonds, (II) trifurcated C–H...O (phenolic) hydrogen bond, (III) O–H (phenolic)...O (carboxylic) hydrogen bond, (IV) C–H(methyl)...O(carboxylic) hydrogen bond, in their decreasing order of interaction energies.

based on high-resolution X-ray charge density analysis⁴⁰. Fluorine atoms in this structure display anisotropy of electron density distribution as seen from the topological features in the interaction region. The magnitude of polarization on fluorine is still not as large compared to its heavier counterparts, but it is safe to assume that for an atom whose size is similar to that of hydrogen, the polarization of the electron cloud is indeed significant. However, it must be stressed that the electron density features of a type II F...F interaction leading to a first experimental visualization of σ -hole on fluorine is observed only in association with a C–F...S interaction (Fig. 8).

15 S...O Chalcogen Bonding in Sulfa Drugs: Multipole Charge Density and X-Ray Wave Function of Acetazolamide

Here is an example of the application of quantum crystallography to unravel the specifics of chalcogen bond formation in acetazolamide⁴¹.

The nature and strength of intra-molecular S...O chalcogen bonds have been characterized using descriptors from the multipole model (MM) and X-ray wave function refinement (XWR). It is interesting to note that routine crystal engineering analysis based on geometrical criteria suggests the possibility of two intra-molecular S...O chalcogen bonded ring motifs, only one satisfies the “orbital geometry” and electron density bond path and a bond critical point criteria. The signatures of aspherical electron density distribution corresponding to the lone pairs and their orientations are seen in the static 3D deformation density map (Fig. 9) ‘ σ -holes’ on the sulfur atom leading to the S...O chalcogen bond as observed on the electrostatic potential surface and Laplacian isosurfaces close to the ‘reactive surface’ (Fig. 10). Table 3 gives the topological parameters derived from both experimental (MM) and theoretical (XWR, Gaussian, G09) analyses clearly bringing out the differences among them which need to be addressed.

Table 1: Comparisons of the BCP properties for intermolecular interactions obtained from experimental charge density model and the corresponding theoretical models.

Interaction	R_{ij} (Å)	d_1 (Å)	d_2 (Å)	ρ ($e \text{ \AA}^{-3}$)	$\nabla^2\rho$ ($e \text{ \AA}^{-5}$)	ϵ	G ($\text{kJ mol}^{-1} \text{ Bohr}^{-3}$)	V ($\text{kJ mol}^{-1} \text{ Bohr}^{-3}$)
O1–H1...O2a	1.6199	1.1024	0.5175	0.39	1.0	0.01	83.51	– 138.72
6-31G**	<i>1.6194</i>	<i>1.0846</i>	<i>0.5348</i>	<i>0.36</i>	<i>2.6</i>	<i>0.01</i>	<i>104.01</i>	<i>– 138.41</i>
TZVP	<i>1.6191</i>	<i>1.0819</i>	<i>0.5372</i>	<i>0.35</i>	<i>3.1</i>	<i>0.00</i>	<i>111.84</i>	<i>– 138.00</i>
O4–H4O...O1b	1.9773	1.2752	0.7022	0.13	1.7	0.23	41.21	– 36.61
6-31G**	<i>1.9784</i>	<i>1.2600</i>	<i>0.7184</i>	<i>0.14</i>	<i>1.9</i>	<i>0.21</i>	<i>44.98</i>	<i>– 39.51</i>
TZVP	<i>1.9747</i>	<i>1.2607</i>	<i>0.7141</i>	<i>0.12</i>	<i>2.2</i>	<i>0.20</i>	<i>50.28</i>	<i>– 39.56</i>
C10–H10c...O2c	2.5184	1.4510	1.0674	0.05	1.0	0.44	19.57	– 12.75
6-31G**	<i>2.4971</i>	<i>1.4456</i>	<i>1.0515</i>	<i>0.05</i>	<i>0.9</i>	<i>0.61</i>	<i>19.29</i>	<i>– 12.82</i>
TZVP	<i>2.5022</i>	<i>1.4379</i>	<i>1.0643</i>	<i>0.05</i>	<i>0.9</i>	<i>0.46</i>	<i>19.08</i>	<i>– 12.60</i>
C2–H2...O4d	2.7680	1.7444	1.0237	0.02	0.3	0.99	6.33	– 3.97
6-31G**	<i>2.7129</i>	<i>1.6128</i>	<i>1.1002</i>	<i>0.03</i>	<i>0.5</i>	<i>0.49</i>	<i>9.68</i>	<i>– 6.43</i>
TZVP	<i>2.7032</i>	<i>1.6076</i>	<i>1.0956</i>	<i>0.03</i>	<i>0.5</i>	<i>0.51</i>	<i>10.05</i>	<i>– 6.38</i>
C5–H5...O4d	2.4898	1.4893	1.0005	0.04	0.9	0.11	17.44	– 11.19
6-31G**	<i>2.4552</i>	<i>1.4580</i>	<i>0.9972</i>	<i>0.05</i>	<i>0.9</i>	<i>0.28</i>	<i>17.98</i>	<i>– 12.49</i>
TZVP	<i>2.4564</i>	<i>1.4551</i>	<i>1.0012</i>	<i>0.05</i>	<i>0.9</i>	<i>0.21</i>	<i>18.07</i>	<i>– 12.21</i>
C10–H10A...O4d	2.4946	1.4933	1.0013	0.05	0.8	0.46	16.80	– 11.16
6-31G**	<i>2.4945</i>	<i>1.4699</i>	<i>1.0247</i>	<i>0.05</i>	<i>0.8</i>	<i>0.29</i>	<i>16.32</i>	<i>– 11.12</i>
TZVP	<i>2.4951</i>	<i>1.4690</i>	<i>1.0261</i>	<i>0.05</i>	<i>0.8</i>	<i>0.26</i>	<i>16.33</i>	<i>– 10.93</i>

Symmetry operations (a) $-x, -y, -z$; (b) $1/2 - x, -1/2 + y, 1/2 - z$; (c) $1/2 - x, -1/2 + y, 1/2 - z$; (d) $1/2 + x, 1/2 - y, 1/2 + z$
Theoretical values are in italics

Table 2: Interaction energies obtained for the molecular dimers (EPMM) and the associated hydrogen bond energies (EHB) calculated from $\rho(\mathbf{r}_b)$ and $\nabla^2\rho(\mathbf{r}_b)$ values (EML)

Interaction	EPMM (kcal mol^{-1})			EML (kcal mol^{-1}) (E_{HB})
	Electrostatic term	Total		
Carboxylic O–H...O dimer				
(Exp)	– 48.27	–	– 33.16	
		47.48		
6-31G**	– 44.11	–	– 33.09	
		43.32		
TZVP	– 36.71	–	– 32.99	
		35.92		
Trifurcated C–H...O dimer				
(Exp)	– 12.45	–	– 3.15	
		15.87		
6-31G**	– 5.68	– 9.09	– 3.59	
TZVP	– 6.14	– 9.55	– 3.53	
Phenolic O–H...O dimer				
(Exp)	– 9.54	–	– 4.38	
		10.77		
6-31G**	– 7.01	– 8.24	– 4.72	
TZVP	– 6.27	– 7.50	– 4.73	
Single C–H...O dimer				
(Exp)	– 0.6	– 1.82	– 1.52	
6-31G**	0.86	– 0.36	– 1.53	
TZVP	– 0.12	– 1.34	– 1.51	

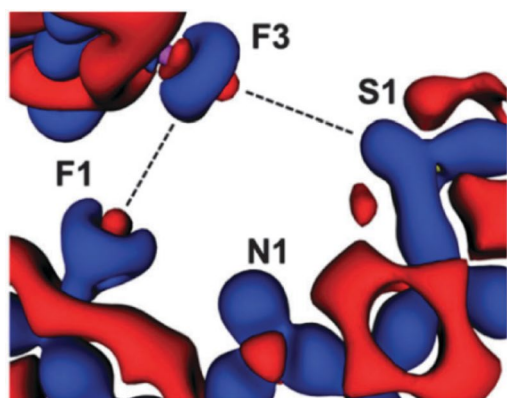
^a Reproduced from the PhD thesis of Sajesh P. Thomas

16 Experimental Proof for the Pnicogen Bond: Cocrystal of 2-Amino-5-Nitropyridine with 2-Chloroacetic Acid

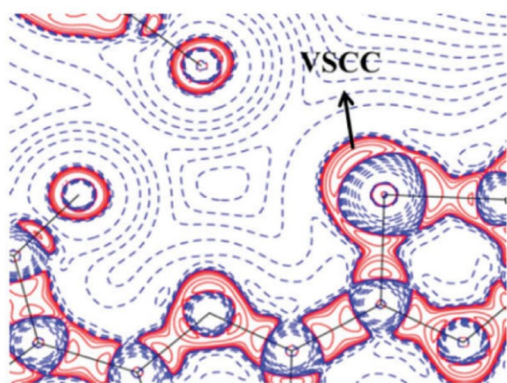
Experimental charge density analysis has proved to be the gold standard to unequivocally establish the existence of the σ -hole and has provided the platform for topological exploration of the bonding aspects. The cocrystal has been designed such that an expected pnicogen bonding will appear in the structure (Fig. 11). The first experimental proof for the existence of a σ -hole on the nitrogen atom, especially when forced into a planar configuration to form a weak but highly directional interaction with a nucleophile resulting in a pnicogen bond is thus demonstrated⁴².

17 'Carbon Bonding' Experimental Evidence from Charge Density Analysis

Mani and Arunan showed based on the atoms in molecule (AIM) calculations on small model molecular systems, unusual bond paths from various nucleophilic atoms to the carbon atom in the $-\text{CH}_3$ group³³. Understanding such a 'carbon bonding' interaction and experimentally validating its existence will offer quantitative evaluation of this interaction and offer insights into the hydrophobic interactions involving hydrocarbons and many organic natural products. Two representative cases were examined (I) the anxiolytic

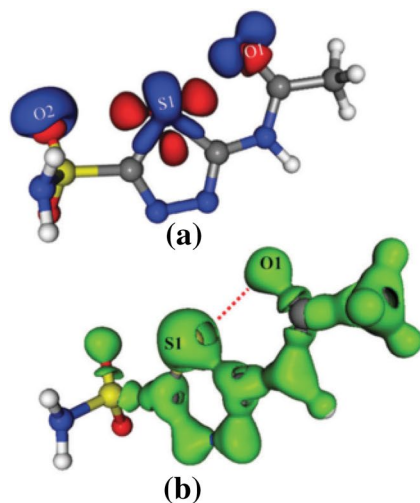


(a)

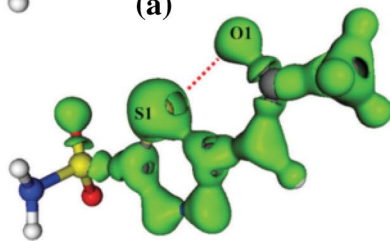


(b)

Figure 8: Experimental **a** $\rho(r)$ and **b** $\Delta^2\rho(r)$ maps in the F... F and S... F interaction region, +ve and -ve values represented by blue and red colors. $\Delta\rho(r)$ isosurfaces are drawn at $0.05 \text{ e } \text{\AA}^{-3}$. $\rho^2(r)$ ($\text{e } \text{\AA}^{-5}$) drawn on the logarithmic scale.



(a)



(b)

Figure 9: **a** Static 3D deformation density ($0.005 \text{ e } \text{\AA}^{-3}$), and **b** Laplacian isosurface map ($1.5 \text{ e } \text{\AA}^{-5}$) from the multipole model refinement. The figure on the right gives Laplacian isosurfaces obtained from X-ray wave function, plotted for $\nabla^2\rho = 0 \text{ e } \text{\AA}^{-5}$, $\nabla^2\rho = -0.1 \text{ e } \text{\AA}^{-5}$.

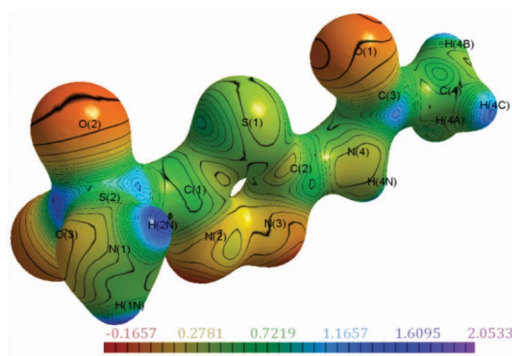


Figure 10: Electrostatic potential isosurface maps obtained from the experimental charge density model of acetazolamide drawn at the isosurface value of $0.5 \text{ e } \text{\AA}^{-3}$. Blue and red colors represent electropositive and electronegative regions, respectively.

drug candidate fenobam for a possible C...Cl carbon bond⁴³, and (II) dimethylammonium 4-hydroxybenzoate for a possible C...O carbon bond (Fig. 11). Compound I exhibited a bond path that originated from the Cl atom and terminated at one of the C-H protons thus indicating that the interaction motif in I is a C-H...Cl hydrogen bond. However, compound II showed a bond path originating from the nucleophilic oxygen atom and terminating at the CH₃ carbon atom with no other bond paths towards C-H hydrogen atoms clearly suggesting a 'carbon bonded' motif (Fig. 12). The 3D deformation density maps clearly bring out the nature of

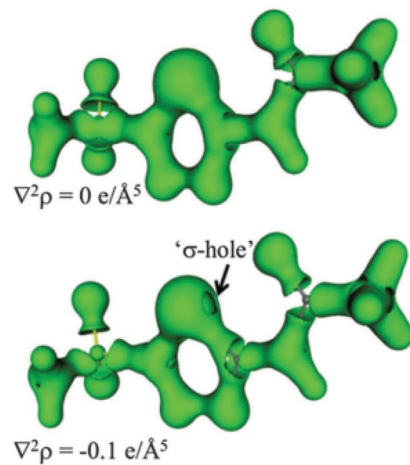
 $\nabla^2\rho = -0.1 \text{ e } \text{\AA}^{-5}$

Table 3: Topological parameters of the S... O chalcogen bond in AZM obtained from the multipole model (MM), X-ray wave function refinement (XWR) and gas phase calculation at the BLYP/def2TZVP level (G09)

	R_{ij} (Å)	d_1 (Å)	d_2 (Å)	ρ ($e \text{ \AA}^{-3}$)	$\nabla^2\rho$ ($e \text{ \AA}^{-5}$)	ϵ
MM	2.7565	1.4421	1.3143	0.123	1.772	0.03
XWR	2.7519	1.4168	1.3351	0.140	0.422	0.23
G09	2.7523	1.4212	1.3311	0.142	0.426	0.23

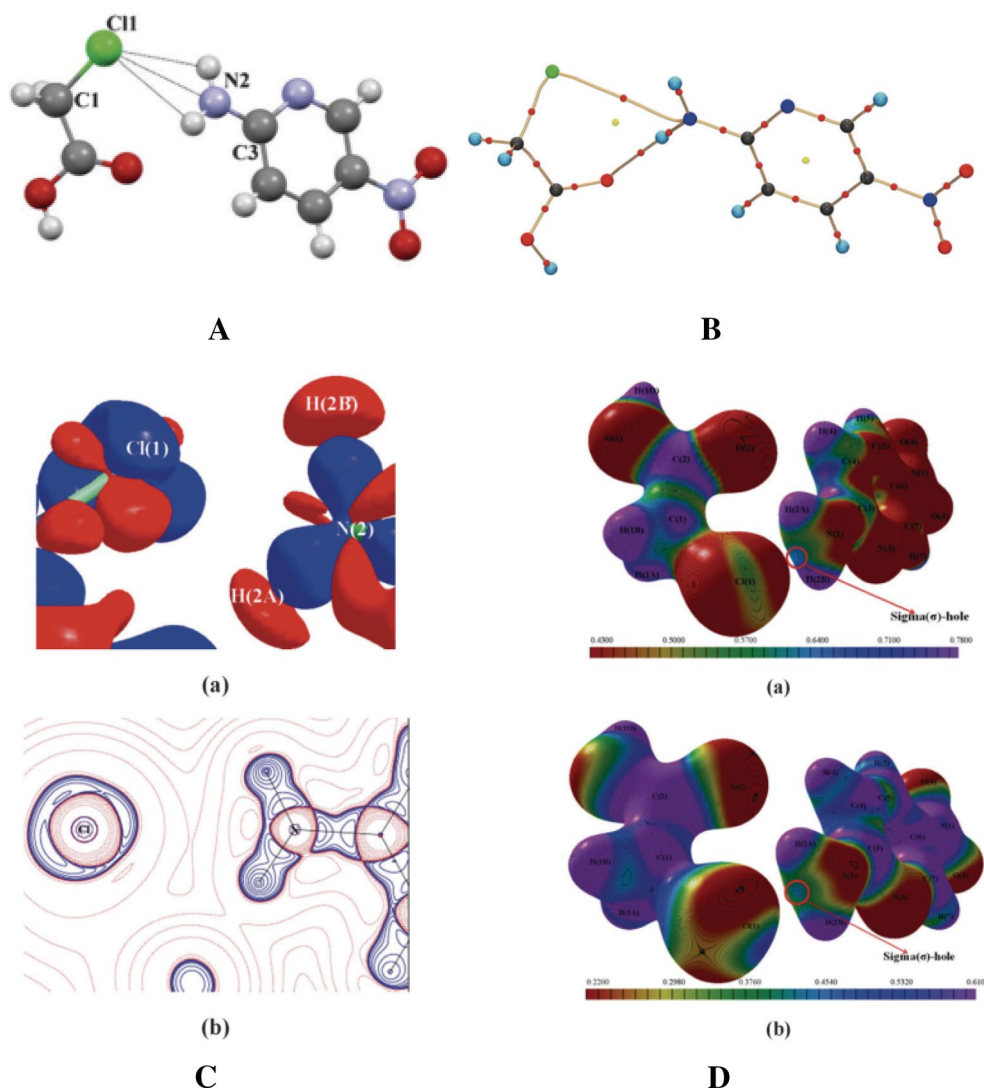


Figure 11: **A** The expected pnictogen bond, **B** the bond path diagram clearly showing the formation of N...Cl interaction, **C a** Experimental 3D deformation density map drawn on an isosurface of $0.08 e \text{ \AA}^3$, **b** 2D Laplacian map drawn at the logarithmic scale. In both cases, +ve and -ve regions are depicted in blue and red, respectively, **D** ESP mapped on the isodensity surface drawn at $0.5 e \text{ \AA}^3$ **a** experiment, **b** theory, showing the possible σ -hole depicted in sky blue. The red part on the color bar indicates an extremely electronegative region, while the violet indicates the relative extreme electropositive region.

bonding in both cases, importantly depicting the σ -holes on the carbon atoms. In II, it is a perfect Politzer-type contact for carbon bonding^{44, 45}. This is a clear example which strongly points out

the study of charge density analysis for understanding the crystal engineering intermolecular contacts to discern the nature of the bonding. Any material design thus will need to adopt the

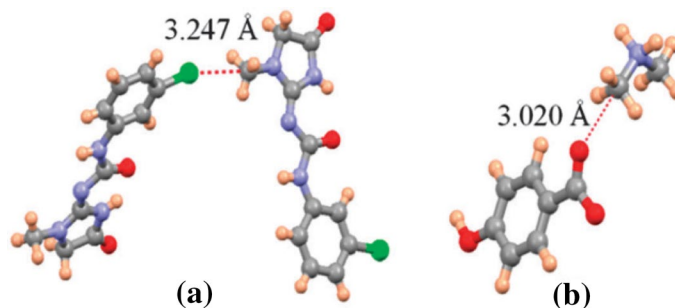


Figure 12: Interaction motifs investigated in this study. **a** Possible C...Cl carbon bonding motif in I and **b** potential C...O carbon bonding motif in II.

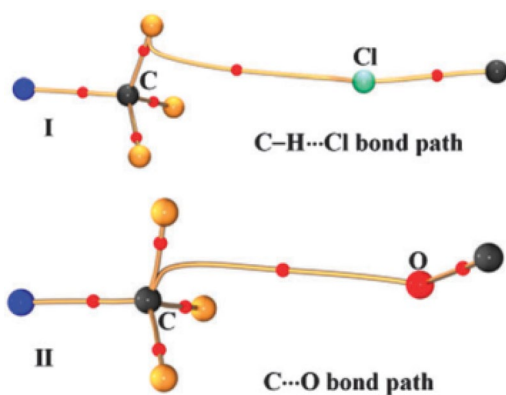


Figure 13: Experimental bond paths together with BCPs in the intermolecular regions of I and II.

quantitative methodology suggested by quantum crystallography (Fig. 13).

18 Insights into the Nature of CH₃...CH₃ Hydrophobic Interactions

The studies on carbon bonding inspired the examination of the ubiquitous hydrophobic interactions which occupy a central stage in most of the biological systems. Understanding these interactions in terms of charge density analysis

allow the visualization of subtle details of electron density features in the interaction region. It is of interest to note that these interactions turn out to be a typical group...group interaction in contrast to σ -hole interactions, which is stabilized by the minimized electrostatic repulsion and maximized dispersion forces⁴⁶. Additionally, for the first time, the solid-state entropic contribution from the torsional mode of the methyl groups in stabilizing these interactions by thermal motion analysis based on neutron diffraction as well as variable temperature crystallography is quantified. A detailed search in the Cambridge Structural Database (CSD) with C...C distance less or equal to the sum of van der Waal radii of C atoms (≤ 3.4 Å) gives 3038 crystal structures (without disorder) containing Me...Me HI motifs, 1840 of these structures have 'face-to-face (3:3)' staggered conformation against 69 hits for 'face-to-face (3:3)' eclipsed conformation between two methyl moieties (Fig. 14). It is noteworthy that the shortest average H...H distance in these Me...Me motifs (both staggered and eclipsed conformation) is found to be higher (2.6776/2.6431 Å) than the sum of van der Waal radii of H atoms (≥ 2.4 Å), whereas the average C...C distance (3.3244/3.3279 Å) is ≤ 3.4 Å. Figure 14 also shows the structures of three

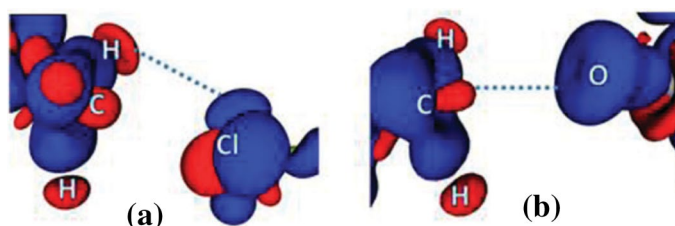


Figure 14: 3D deformation density maps in **a** the C-H...Cl interaction region in I and **b** the C...O carbon bonding region in II. Red regions represent CD and blue regions represent CC. The $\nabla^2\rho$ isosurfaces are drawn at ± 0.02 e Å⁻³.

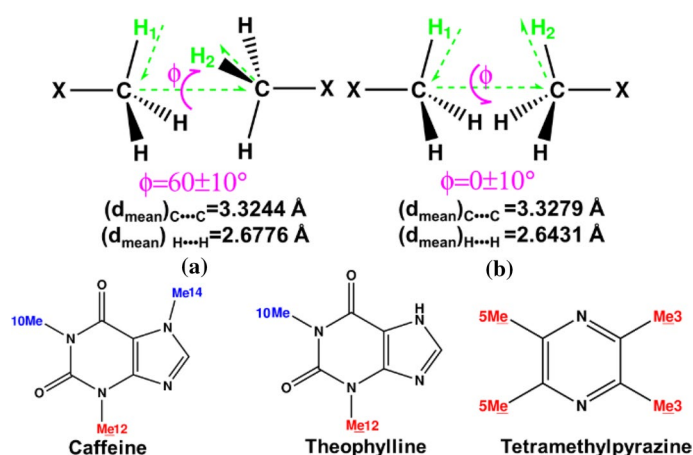


Figure 15: **a** 'Face-to-face' (3:3) staggered intermolecular conformation and **b** 'face-to-face' (3:3) eclipsed intermolecular conformation between methyls. ϕ is the dihedral angle between $\text{H}_1\text{-C}\cdots\text{C}$ and $\text{H}_2\text{-C}\cdots\text{C}$ plane, $(d_{\text{mean}})_{\text{C}\cdots\text{C}}$ is the mean intermolecular $\text{C}\cdots\text{C}$ distances, $(d_{\text{mean}})_{\text{H}\cdots\text{H}}$ is the shortest intermolecular $\text{H}\cdots\text{H}$ distances (top). Molecular diagram of active pharmaceutical ingredient (API) molecules containing the HI methyl groups (red) and non-HI methyl groups (blue) (bottom).

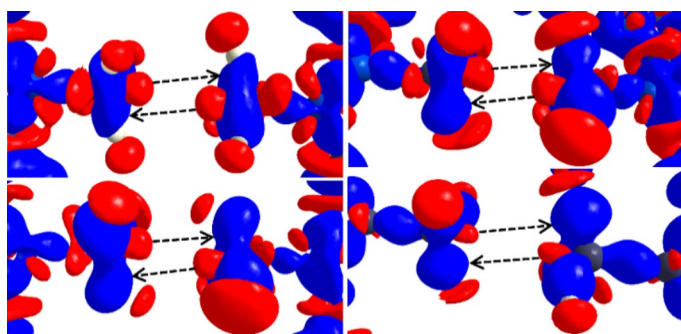


Figure 16: Experimental 3D deformation density map drawn on isosurface of $\pm 0.08 \text{ e} \text{ \AA}^{-3}$. Blue represents charge concentration and red represents charge depletion regions, respectively. Caff-3HNA (top left), Caff-PZCA (top right), Theo-25DFBZA (bottom left), TMP-OA (Me3) (bottom right).

conformers in the crystal structures subjected to charge density analysis. The cocrystals examined are caffeine:3-hydroxy-2-naphthoic acid (Caff-3HNA), caffeine:3,5-pyrazoledicarboxylic acid (Caff-PZCA), theophylline:2,5-difluorobenzoic acid (Theo-25DFBZA) and 2,3,5,6-tetramethylpyrazine: oxalic acid (TMP-OA).

Multipole analysis based on high-resolution X-ray diffraction data of all four compounds show the charge depleted positive sigma holes (red lobes) along the C-X bond direct towards each other (Fig. 15). A 'misalignment' is observed in the relative positioning of the sigma holes (i.e., $\text{X-C}\cdots\text{C-X}$ bonds are not collinear in the $\text{Me}\cdots\text{Me}$ region). This causes the δ^+ sigma holes to get partly exposed to the δ^- C-H bonding pair (blue lumps; as indicated by the black arrows) reducing the electrostatic repulsion between the methyl groups.

The bond path diagram (Fig. 16) brings out the nature of group...group interactions with a lack of directionality clearly indicating that hydrophobic interactions are entirely different from any conventional σ -hole bonding or donor-acceptor interactions. Further, it is established that methyl groups display larger atomic displacement parameters (ADPs) and is shown to be due to the influence of torsional entropy based on variable temperature diffraction studies. This observation is expected to have significant impact on biological systems (Fig. 17).

19 Conclusions

The classification of the variety of interactions involving elements from the Group 14–17 of the periodic table in terms of their topological properties has firmly established the role of σ -holes

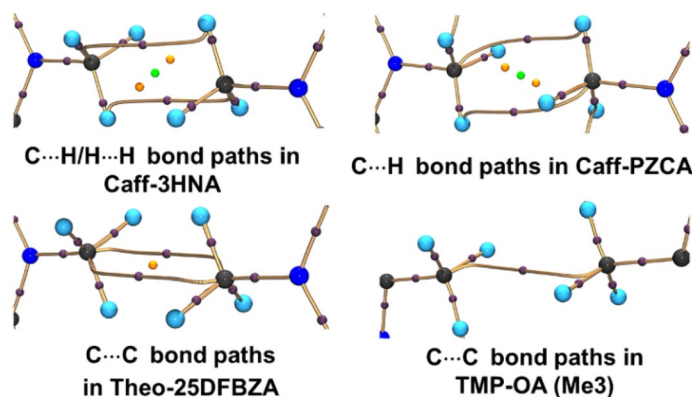


Figure 17: Bond paths along with critical points of hydrophobic Me...Me interactions. The violet, orange and the green spheres represent the (3, - 1) bond critical points (BCPs), (3, +1) ring critical points (RCPs) and (3, +3) cage critical points (CCPs).

which allow for the polarization of the electron density with specific directional preferences. The relative strengths of such intermolecular interactions estimated by experimental and theoretical charge density analysis suggest the design and fabrication aspects of molecular materials. The recent results on the nature of hydrophobic interactions will have a significant impact in explaining hitherto inaccessible biological functions and drug action. In general, charge density analysis on molecular crystals provides a pristine evaluation of intermolecular interactions and hence has a major impact on the area of quantitative crystal engineering. The identification of synthons as building blocks based on routine crystal structure analysis made significant inroads to design specific engineered molecule, however, the results from quantum crystallography as demonstrated in this mini-review provide the functionality to the tools of crystal engineering to be utilized in design and fabrication of molecules with the desired properties.

Publisher's Note

Springer Nature remains neutral with regard to jurisdictional claims in published maps and institutional affiliations.

Acknowledgements

The work reported in this review was mainly carried out by my students and post-doctoral associates in my group. I should specifically acknowledge the contributions from Drs. Parthapratim Munshi, Venkatesha Hathwar, Sajesh P. Thomas, Mysore S. Pavan, Sounak Sarkar who essentially contributed to the contents of this article. I would like to thank Indian Institute of

Science and DST, India for the funding to procure the X-ray facility. I also acknowledge the funding provided under the J.C. Bose fellowship by DST, India.

Received: 5 November 2019 Accepted: 2 December 2019

Published online: 27 December 2019

References

- Desiraju GR, Vittal JJ, Ramanan A (2012) Crystal engineering: a textbook. World Scientific Publishing Company Incorporated, Singapore
- Koritsanszky TS, Coppens P (2001) Chemical applications of X-ray charge-density analysis. *Chem Rev* 101(6):1583
- McKinnon JJ, Spackman MA, Mitchell AS (2004) Novel tools for visualizing and exploring intermolecular interactions in molecular crystals. *Acta Crystallogr Sect B* 60:627
- Krawczuk A, Macchi P (2014) Charge density analysis for crystal engineering. *Chem Cent J* 8(1):68
- Hansen NK, Coppens P (1978) Testing aspherical atom refinements on small-molecule data sets. *Acta Crystallogr Sect A* 34:909
- Koritsanszky T et al (2015) XD2015—a computer program package for multipole refinement, topological analysis of charge densities and evaluation of intermolecular energies from experimental and theoretical structure factors. University at Buffalo, State University of New York, NY, USA
- Frisch M et al (2009) Gaussian 09, revision a. 02. Gaussian Inc., Wallingford, CT, p 200
- Dovesi R et al (2017) CRYSTAL17 user's manual. Università di Torino, Torino
- Jayatilaka D, Grimwood DJ (2001) Wavefunctions derived from experiment. I. Motivation and theory. *Acta Crystallogr Sect A* 57(1):76

10. Capelli SC et al (2014) Hirshfeld atom refinement. *IUCr* 1(5):361
11. Malaspina LA, Wieduwilt EK, Bergmann J, Kleemiss F, Meyer B, Ruiz-López MF, Pal R, Hupf E, Beckmann J, Piltz RO, Edwards AJ, Grabowsky S, Genoni A (2019) Fast and accurate quantum crystallography: from small to large, from light to heavy. *J Phys Chem Lett* 10:6973
12. Massa L, Huang L, Karle J (1995) Quantum crystallography and the use of kernel projector matrices. *Int J Quantum Chem* 56(S29):371
13. Clinton WL, Galli AJ, Massa LJ (1969) Direct determination of pure-state density matrices. II. construction of constrained idempotent one-body densities. *Phys Rev* 177(1):7
14. Tanaka K et al (2008) X-ray atomic orbital analysis. I. Quantum-mechanical and crystallographic framework of the method. *Acta Crystallogr Sect A* 64(4):437
15. Coppens P, Guru Row TN, Leung P, Stevens ED, Becker PJ, Yang YW (1979) Net atomic charges and molecular dipole moments from spherical-atom X-ray refinements, and the relation between atomic charge and shape. *Acta Crystallogr Sect A* 35:63
16. Bader RFW (1990) *Atoms in molecules*. Wiley, New York
17. Desiraju GR (1995) Supramolecular synthons in crystal engineering—a new organic synthesis. *Angew Chem Int Ed Engl* 34:2311
18. Desiraju GR (1997) Designer crystals: intermolecular interactions, network structures and supramolecular synthons. *Chem Commun* 16:1475
19. Nangia A, Desiraju GR (1998) Design of organic solids. In: Weber E (ed) *Perspectives in supramolecular chemistry*. Springer, Berlin, pp 57–95
20. Etter MC (1990) Encoding and decoding hydrogen-bond patterns of organic compounds. *Acc Chem Res* 23:120
21. Steiner T (2003) O hydrogen bonding in crystals. *Cryst Rev* 9(2–3):177
22. Koch U, Popelier PLA (1995) Characterization of C–H–O hydrogen bonds on the basis of the charge density. *J Phys Chem* 99:9747
23. Munshi P, Guru Row TN (2002) Electron density study of 2H-chromene-2-thione. *Acta Crystallogr Sect B* 58:1011
24. Mallinson PR, Smith GT, Wilson CC, Grech E, Wozniak KJ (2003) From weak interactions to covalent bonds: a continuum in the complexes of 1,8-Bis(dimethylamino)naphthalene. *J Am Chem Soc* 125:4259
25. Munshi P, Guru Row TN (2005) Exploring the lower limit in hydrogen bonds: analysis of weak C–H...O and C–H... π interactions in substituted coumarins from charge density analysis. *J Phys Chem A* 109:659
26. Politzer P, Murray JS, Clark T (2013) Halogen bonding and other σ -hole interactions: a perspective. *Phys Chem Chem Phys* 15(27):11178
27. Desiraju GR et al (2013) Definition of the halogen bond (IUPAC Recommendations 2013). *Pure Appl Chem* 85(8):1711
28. Williams D, Hsu LY (1985) New analytical scattering-factor functions for free atoms and ions. *Acta Crystallogr Sect A* 41:296
29. Nyburg SC, Wong-Ng W (1979) Anisotropic atom–atom forces and the space group of solid chlorine. *Proc R Soc Lond A* 367:29
30. Desiraju GR, Parthasarathy R (1989) The nature of halogen.cntdot..cntdot..cntdot.halogen interactions: are short halogen contacts due to specific attractive forces or due to close packing of nonspherical atoms? *J Am Chem Soc* 111(23):8725
31. Rosenfield RE Jr, Parthasarathy R, Dunitz JDJ (1977) Directional preferences of nonbonded atomic contacts with divalent sulfur. 1. Electrophiles and nucleophiles. *J Am Chem Soc* 99(14):4860
32. Guru Row TN, Parthasarathy R (1981) Directional preferences of nonbonded atomic contacts with divalent sulfur in terms of its orbital orientations. 2. Sulfur.cntdot..cntdot..sulfur interactions and nonspherical shape of sulfur in crystals. *J Am Chem Soc* 103(2):477
33. Mani D, Arunan E (2013) The X–CY (X = O/F, Y = O/S/F/Cl/Br/N/P) ‘carbon bond’ and hydrophobic interactions. *Phys Chem Chem Phys* 15(34):14377
34. Desiraju G, Steiner T (1999) *The weak hydrogen bond*. In *Structural Chemistry and Biology*. Oxford University Press, Oxford
35. Volkov A, Koritsanszky T, Coppens P (2004) Combination of the exact potential and multipole methods (EP/MM) for evaluation of intermolecular electrostatic interaction energies with pseudoatom representation of molecular electron densities. *Chem Phys Lett* 391:170
36. Thomas SP, Pavan MS, Guru Row TN (2012) Experimental evidence for ‘carbon bonding’ in the solid state from charge density analysis. *Cryst Growth Des* 12:6083
37. Thalladi VR, Weiss H-C, Bläser D, Boese R, Nangia A, Desiraju GR (1998) C–H...F Interactions in the crystal structures of some fluorobenzenes. *J Am Chem Soc* 120:8702
38. Metrangolo P, Murray JS, Pilati T, Politzer P, Resnati G, Terraneo G (2011) Fluorine-centered halogen bonding: a factor in recognition phenomena and reactivity. *Cryst Growth Des* 11:4238
39. Hathwar VR, Guru Row T (2011) Charge density analysis of heterohalogen (Cl...F) and homohalogen (F...F) intermolecular interactions in molecular crystals: importance of the extent of polarizability. *Cryst Growth Des* 11:1338
40. Pavan MS, Prasad KD, Guru Row TN (2013) Halogen bonding in fluorine: experimental charge density study on intermolecular F...F and F...S donor–acceptor contacts. *Chem Commun* 49:7558
41. Thomas SP, Jayatilaka D, Guru Row TN (2015) S...O chalcogen bonding in sulfa drugs: insights from multipole charge density and X-ray wavefunction of acetazolamide. *Phys Chem Chem Phys* 17:25411

42. Sarkar S, Pavan MS, Guru Row TN (2015) Experimental validation of 'pnictogen bonding' in nitrogen by charge density analysis. *Phys Chem Chem Phys* 17:2330
43. Thomas SP, Nagarajan K, Guru Row TN (2012) Polymorphism and tautomeric preference in fenobam and the utility of NLO response to detect polymorphic impurities. *Chem Commun* 48:10559
44. Bundhun A, Ramasami P, Murray J, Politzer P (2013) Trends in σ -hole strengths and interactions of F3MX molecules (M = C, Si, Ge and X = F, Cl, Br, I). *J Mol Model* 19:2739
45. Thomas SP, Pavan MS, Guru Row TN (2014) Experimental evidence for 'carbon bonding' in the solid state from charge density analysis. *Chem Commun* 50:49
46. Sarkar S, Thomas SP, Lokeswara Rao P, Edwards AJ, Grosjean A, Ramanathan KV, Guru Row TN (2019) Experimental insights into the electronic nature, spectral features, and role of entropy in short $\text{CH}_3 \cdots \text{CH}_3$ hydrophobic interactions. *J Phys Chem Lett* 10(22):7224



Professor T. N. Guru Row is currently an honorary professor at Solid State and Structural Chemistry Unit of the the Indian Institute of Science, Bangalore. He is also an INSA Senior Scientist at present. He completed his B.Sc (Hons) and M.Sc from Bangalore University and Ph.D. from the Indian Institute of Science. He has served as Dean (Science Faculty) of the IISc and was the Editor-in-Chief of the Journal of Indian Institute of Science till 2017. His major area of research has been chemical crystallography and materials design which include charge density analysis in molecular crystals, intermolecular interactions, hydrogen bonding, halogen bonding and other

weak interactions, phase transitions in complex inorganic systems with emphasis on mineral evolution and generation of futuristic materials, structural aspects of polymorphism, co-crystals, salts and eutectics in pharmaceuticals, in situ cryo-crystallography and protein expression, purification and crystallization. He is a fellow of the Indian Academy of Sciences, Indian National Science Academy, the Royal Society of Chemistry and International Center for Diffraction Data, USA. He has been a recipient of J.C. Bose National fellowship and has been awarded IISc Alumni award of excellence in science.